Supplementary Information

A Cell Metamodel Uncovers Mechanistic Drivers of Disease Phenotypes Across Molecular, Cellular, and Tissue Scales

Chenxi Wang[1,2,*], Jingjing Zheng[1,2,*], Weimin Li[3], Xianni Zhong[1,2], Bing Yu[1,2], Angdi Li[1], Junjie He[4], Xiaoyan Liu[1], Qifeng Liao[4], Andrej Sali[5,6], Xuming He[4,7,†], Liping Sun[1,†]

[1]iHuman Institute, ShanghaiTech University, Shanghai 201210, China
[2]School of Life Science and Technology, ShanghaiTech University, Shanghai 201210, China
[3]National Key Laboratory of Biomacromolecules, CAS Center for Excellence in Biomacromolecules, Institute of Biophysics, Chinese Academy of Sciences, Beijing, China
[4]School of Information Science and Technology, ShanghaiTech University, Shanghai 201210, China
[5]Department of Bioengineering and Therapeutic Sciences, University of California, San Francisco, CA 94158
[6]Quantitative Biosciences Institute, University of California, San Francisco, CA 94158
[7]Shanghai Engineering Research Center of Intelligent Vision and Imaging, Shanghai 201210, China

[*]**Corresponding authors:**
Liping Sun: sunlp@shanghaitech.edu.cn;
Xuming He: hexm@shanghaitech.edu.cn.

Supplementary information includes supplementary text, seven supplementary figures, and three supplementary tables.

Supplementary Text

1. Input models and their corresponding surrogate models

1.1 Vesicle Exocytosis (VE) model

Input model. The vesicle exocytosis (VE) model [1] is an ODE-based model that describes the formation of insulin vesicles, their dynamics across four distinct pools (*ie*, the reserve pool, N_R^{VE}, the immediately releasable pool, N_{IR}^{VE}, the docked pool, N_D^{VE}, and the fused pool, N_F^{VE}, as well as their exocytosis. Model variables and parameters are provided in Table S1, and the model equations are:

$$
\begin{aligned}
\dot{I}(t) &= -kI(t)V(t) - \alpha_I I(t) + b_I \\
\dot{V}(t) &= -kI(t)V(t) - \alpha_V V(t) + b_V + \sigma N_F(t - \tau_V) \\
\dot{R}(t) &= kI(t)V(t) - \gamma R(t) \\
\dot{N_D}(t) &= \gamma N_R(t) - k_1^+[C_T - N_{IR}(t)]N_D(t) + k_1^- N_{IR}(t) \\
\dot{N_{IR}}(t) &= k_1^+[C_T - N_{IR}(t)]N_D(t) - k_1^- N_{IR}(t) - \rho N_{IR}(t) \\
\dot{N_F}(t) &= \rho N_{IR}(t) - \sigma N_F(t) \\
\dot{\gamma}(t) &= \eta\{-\gamma(t) + \gamma_b + \Phi(t) + h_\gamma[G(t - \tau_G)]\} \\
\dot{\rho}(t) &= \zeta\{-\rho(t) + \rho_b + h_\rho[\gamma(t)]\} \\
h_\gamma(G) &= \begin{cases} 0, & G \le G^* \\ \frac{\hat{h} - (G - G^*)}{\hat{G} - G^*} & G^* < G \le \hat{G} \\ \hat{h}, & G > \hat{G} \end{cases} \\
h_\rho(\gamma) &= \begin{cases} 0, & \gamma < \gamma_b \\ k_\rho(\gamma - \gamma_b), & \gamma \ge \gamma_b \end{cases} \\
S(t) &= I_0 \sigma N_F(t) f[G(t - \tau_G)]
\end{aligned}
$$

Surrogate model. The surrogate VE model is constructed with a time step of 10^{-4} minutes, ensuring an optimal balance between computational efficiency and numerical stability. The process model adapts the ODEs of the VE input model as forward functions without simplification. The observation model is formulated based on experimental data or, in its absence, an identical function to maintain consistency between predicted and observed states. Transition and emission noises are time-variant, defined as 10^{-3} and 10^{-2} of the respective mean values of the surrogate model variables at each time step.

1.2 Insulin Secretion Kinetic (ISK) model

Input model. The insulin secretion kinetic (ISK) model [2] employs a two-compartment representation to describe Ca^{2+} distributions in the cytosol, Ca_{ic}^{ISK}, and in the Ca^{2+} microdomains near the voltage-sensitive Ca^{2+} channels, Ca_{md}^{ISK}, as well as the Ca^{2+}-dependent insulin secretion kinetics of a single β-cell. Model

variables and parameters are provided in Table S2, and the model equations are:

$$
\begin{aligned}
\dot{Ca_{md}}(t) &= f_{md}J_L(t) - f_{md}B[Ca_{md}(t) - Ca_{ic}(t)] \\
\dot{Ca_{ic}}(t) &= f_i J_R(t) - f_v f_i B[Ca_{md}(t) - Ca_{ic}(t)] - f_i L(Ca_{ic}(t)) \\
J_L(t) &= \frac{-\alpha J_L(t)}{v_{md}} \\
J_R(t) &= \frac{-\alpha J_R(t)}{v_{cell}} \\
\dot{N_1}(t) &= -[3k_1 Ca_{md}(t) + r_{-1}]N_1(t) + k_{-1}N_2(t) + r_1 N_5(t) \\
\dot{N_2}(t) &= 3k_1 Ca_{md}(t)N_1(t) - [2k_1 Ca_{md}(t) + k_{-1}]N_2(t) + 2k_{-1}N_3(t) \\
\dot{N_3}(t) &= 2k_1 Ca_{md}(t)N_2(t) - [k_1 Ca_{md}(t) + 2k_{-1}]N_3(t) + 3k_{-1}N_4(t) \\
\dot{N_4}(t) &= k_1 Ca_{md}(t)N_3(t) - [3k_{-1} + \mu_1]N_4(t) \\
\dot{N_5}(t) &= r_{-1}N_1(t) - [r_1 + r_{-2}]N_5(t) + r_2 N_6(t) \\
\dot{N_6}(t) &= r_3 + r_{-2}N_5(t) - [r_{-3} + r_2]N_6(t)
\end{aligned}
$$

$$
\begin{aligned}
\dot{N_F}(t) &= \mu_1 N_4(t) - \mu_2 N_F(t) \\
\dot{N_R}(t) &= \mu_2 N_F(t) - \mu_3 N_R(t) \\
N_S(t) &= \int_0^t \mu_3 N_R(t')dt' \\
S &= I_0 \sigma N_F(t)
\end{aligned}
$$

Surrogate model. The surrogate ISK model is constructed with a time step of 10^{-5} minutes. The process model adapts the ODEs of the ISK input model as forward functions without simplification, except for the variable S_{islet}^{ISK} , which requires additional interpolation based on the number of secreted vesicles, N_S^{ISK}, after solving the ODEs. The observation model is formulated based on experimental data or, in its absence, an identical function. Transition and emission noises are time-variant, defined as 10^{-2} and $2*10^{-1}$ of the respective mean values of surrogate model variables at each time step.

1.3 Islet Cell Network (ICN) model

Input model. The islet network (ICN) model [3] is a network model that describes the electrical dynamics, V_{mem}^{ICN}, and Ca^{2+} dynamics, Ca_{ic}^{ICN}, of individual β cells within the islet during insulin secretion. The model employs hexagonal closest packing to construct an islet network of β-cells, simulating intercellular communication mediated by gap junctions, K_{ATP} channels, Ca^{2+} channels, as well as Ca^{2+} and Cl^- pumps. Model variables and parameters are provided in Table S3, and the model equations are:

$$
\begin{aligned}
-C_M\dot{V_i} &= I_{katp}(V_i) + I_{ca}(V_i) + I_k(V_i, n_i) + I_s(V_i, s_i) + I_{coup}(V_i) + I_{cl}(V_i) \\
\dot{n_i} &= \frac{n_\infty(V_i) - n_i}{\tau_n} \\
\dot{s_i} &= \frac{s_\infty(V_i) - s_i}{\tau_s} \\
\dot{Ca_i} &= f[-\alpha I_{ca}(V_i) - k_{ca,i}] \\
I_{katp}(V_i) &= g_{katp}(V_i - V_k) \\
I_{ca}(V_i) &= g_{ca} m_\infty(V_i)(V_i - V_{ca}) \\
I_k(V_i, n_i) &= g_k n_i (V_i - V_k) \\
I_s(V_i, s_i) &= g_s s_i (V_i - V_k) \\
I_{coup}(V_i) &= \sum_{j \in N(i)} g_{c_i,j}(V_i - V_j) \\
I_{cl}(V_i) &= g_{cl}\sigma(V_i - V_{cl})
\end{aligned}
$$

Surrogate model. The surrogate ICN model is constructed with a time step of $5*10^{-4}$ minutes. The process model adapts the ODEs of the ICN input model as forward functions without simplification. The observation model is formulated based on experimental data or, in its absence, an identical function. Transition and emission noises are time-variant, defined as 10^{-3} and 10^{-1} of the respective mean values of surrogate model variables at each time step.

2. Estimation of model joint distribution

For input models lacking inherent uncertainty (*eg*, ODE models), variable distributions were estimated based on the experimental data used during model construction. Each variable was assumed to follow a Gaussian distribution characterized by a mean, μ and a standard deviation, σ. For time points with experimentally determined mean and SD values, these were directly assigned as μ and σ. In case of incomplete data, an average percentage, p_σ, was calculated as the ratio of the SD to the corresponding mean of the experimental data at available time points. For time points where only the mean was known, μ was set to the experimental mean, and σ was determined as the absolute difference between the experimental mean and the corresponding model-derived mean. This is justified by the generally good fit of ODE models, as evidenced by the model-derived mean falling within the experimental SD. For time points lacking both mean and SD, μ was set to the model-derived variable mean, and σ was estimated as μ multiplied by p_σ, where p_σ was derived from the available data points. The model's joint distribution is thus estimated based on experimental data, with robust approximations for missing values.

3. Validation of graph-based metamodeling using a synthetic benchmark

Toy system. We construct a toy system of glucose-stimulated insulin secretion to describe the dynamics of five variables over 7 minutes: glucose intake from food digestion, D, intracellular glucose level, G, β-cell activity, γ, insulin secretion rate of a β-cell, S_{cell}, and insulin secretion rate of an islet, S_{islet} (SI Fig. S3A). These dynamics are governed by five nonlinear Ordinary Differential Equations (ODEs):

$$\begin{aligned}
\frac{dG}{dt} &= \beta_1 S_{cell} + \beta_2(\gamma)^{\frac{2}{3}} + \beta_3 \\
\frac{dS_{cell}}{dt} &= \beta_4\gamma + \beta_5 S_{cell} + \beta_6 \\
\frac{d\gamma}{dt} &= \beta_7(S_{cell})^2 + \beta_8 \\
\frac{dD}{dt} &= \alpha_1 \ln(S_{islet}) + \alpha_2 \\
\frac{dS_{islet}}{dt} &= \alpha_3(D)^2 + \alpha_4 D + \alpha_5
\end{aligned}$$

Each variable is assigned a 15% uncertainty, serving as the Truth. The toy system is then divided into two subsystems, referred to as the Cell and Body subsystems. Simulated experimental data are generated by introducing random noise to the Truth of each variable. Input models for the subsystems are constructed by fitting the parameters of the corresponding ODEs to the simulated data using linear regression.

Input models. The input Cell model describes the dynamics of the intracellular glucose level, G^C, insulin secretion rate, S^C, and cell activity, γ^C, on a timescale of 0.01 minutes, using three ODEs:

$$\begin{aligned}
\frac{dG^C}{dt} &= \beta_1 S^C + \beta_2(\gamma^C)^{\frac{2}{3}} + \beta_3 \\
\frac{dS^C}{dt} &= \beta_4\gamma^C + \beta_5 S^C + \beta_6 \\
\frac{d\gamma^C}{dt} &= \beta_7(S^C)^2 + \beta_8
\end{aligned}$$

The input Body model describes the dynamics of insulin secretion rate of an islet, S^B, in response to the

glucose uptake from food digestion, D^B, on a timescale of 0.05 minutes, using two ODEs:

$$\frac{dD^B}{dt} = \alpha_1 \ln(S^B) + \alpha_2$$
$$\frac{dS^B}{dt} = \alpha_3 (D^B)^2 + \alpha_4 D^B + \alpha_5$$

Surrogate models. The surrogate Cell and Body models are constructed with time steps of 0.01 and 0.05 minutes, respectively. The process model adapts the ODEs as forward functions, while the observation model uses the simulated experimental data as observations. Joint distributions of the input and surrogate Body models largely overlap, validating the conversion step (SI Fig. S3B).

Metamodel. Two surrogate models with varying timesteps (Cell: 0.01 min; Body: 0.05 min) are redefined to the universal time step of 0.01 min. The Cell surrogate model required no redefinition, as its timestep already matches the universal timestep. For the Body surrogate model, the process model was redefined using an ODE solver at the universal timestep; the observation model was computed through interpolation of the simulated experimental data. The connecting variables, S^C and S^B, are selected by comparing the Pearson correlation coefficient for all pairs of surrogate model variables (SI Fig. S3C). The coupling variable S^c_{cell} is introduced, with its prior distribution defined as a mixture function of the connecting variable distributions with equal weights. To establish their statistical dependencies, two edges are introduced from the coupling variable to the connecting variables $S^C \leftarrow S^c_{cell} \rightarrow S^B$ (SI Fig. S3D), with conditional distributions, $P(S^C|S^c_{cell})$, $P(S^B|S^c_{cell})$, defined as:

$$P(S^B_{t+1}|S^c_{cell,t}, S^B_t) = N([\omega_1 S^c_{cell,t} + (1-\omega_1) f^B(S^B_t, D^B_t)], \phi^1_t),$$
$$P(S^C_{t+1}|S^c_{cell,t}, S^C_t) = N([\omega_2 S^c_{cell,t} + (1-\omega_2) f^C(S^C_t, \gamma^C_t, G^C_t)], \phi^2_t)$$

where ω_1 and ω_2 are weights determined by the relative overlaps between the coupling variable distribution and the connecting variable distributions. Metamodel inference was performed using both the Unscented Kalman Filter (UKF) and the Particle Filter (PF), yielding comparable accuracy, with the PF exhibiting smaller uncertainty as expected (SI Fig. S3E). We also integrate two input models using widely adopted Common Timestep Integration (CTI) approach [4] to evaluate changes in model accuracy before and after integration. As a result, graph-based metamodeling achieves superior accuracy compared to both the input models and the CTI approach (SI Fig. S3F). The synthetic metamodel is available on Github https://github.com/SunLab-SH/GraphMM.

References

[1] Bertuzzi, A., Salinari, S. & Mingrone, G. Insulin granule trafficking in β-cells: mathematical model of glucose-induced insulin secretion. *American Journal of Physiology-Endocrinology and Metabolism* **293**, E396–E409 (2007).

[2] Wang, S., Sherman, A. *et al.* Identifying the targets of the amplifying pathway for insulin secretion in pancreatic β-cells by kinetic modeling of granule exocytosis. *Biophysical journal* **95**, 2226–2241 (2008).

[3] Hogan, J. P. & Peercy, B. E. Flipping the switch on the hub cell: Islet desynchronization through cell silencing. *PloS one* **16**, e0248974 (2021).

[4] Agmon, E. *et al.* Vivarium: an interface and engine for integrative multiscale modeling in computational biology. *Bioinformatics* **38**, 1972–1979 (2022).

Supplementary Figures

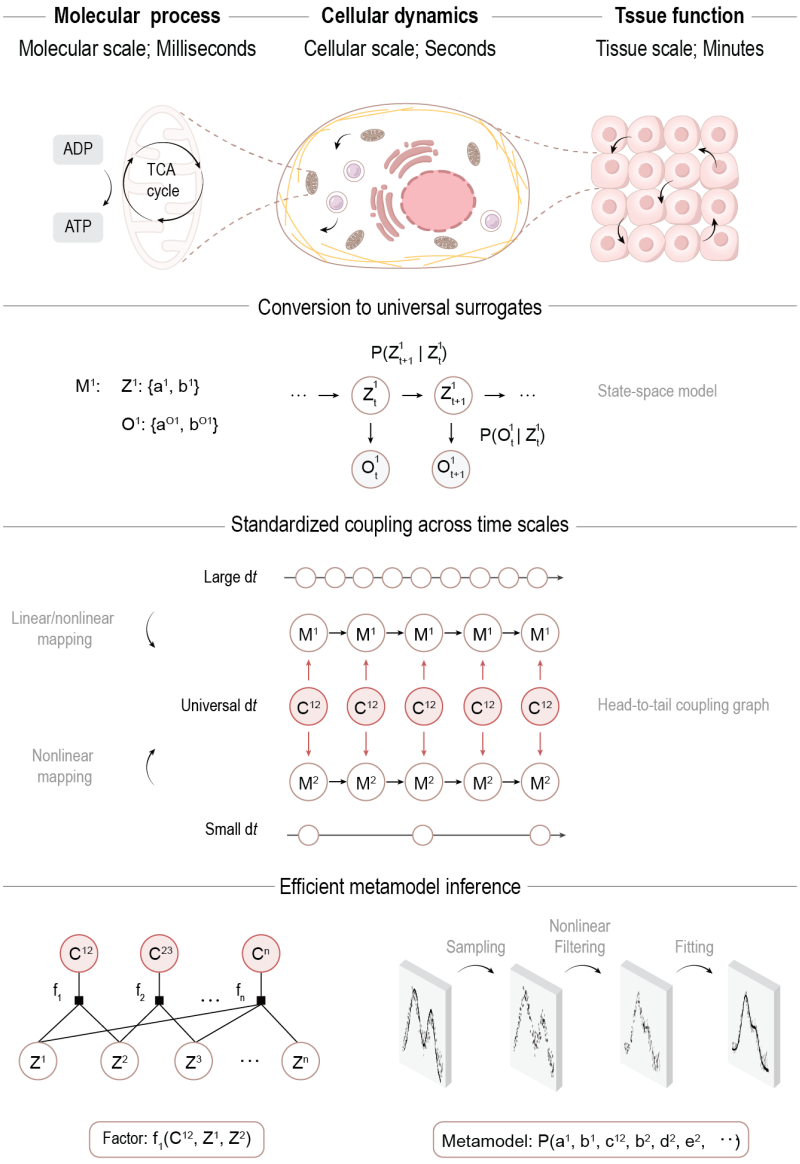

Fig. S1 The top panel illustrates three diverse input models: molecular signaling pathways (milliseconds), cellular components and dynamics (seconds), and multicellular communications (minutes). The middle panel outlines three metamodeling stages: (i) unifying representations of diverse inputs using state space models; (ii) standardized coupling across timescales using nonlinear and linear mappings to unify temporal resolutions, followed by constructing coupling PGM graph using a standardized strategy; and (iii) efficient metamodel inference employing factor graphs and Kalman Filters (KFs) for estimating model variable distributions.

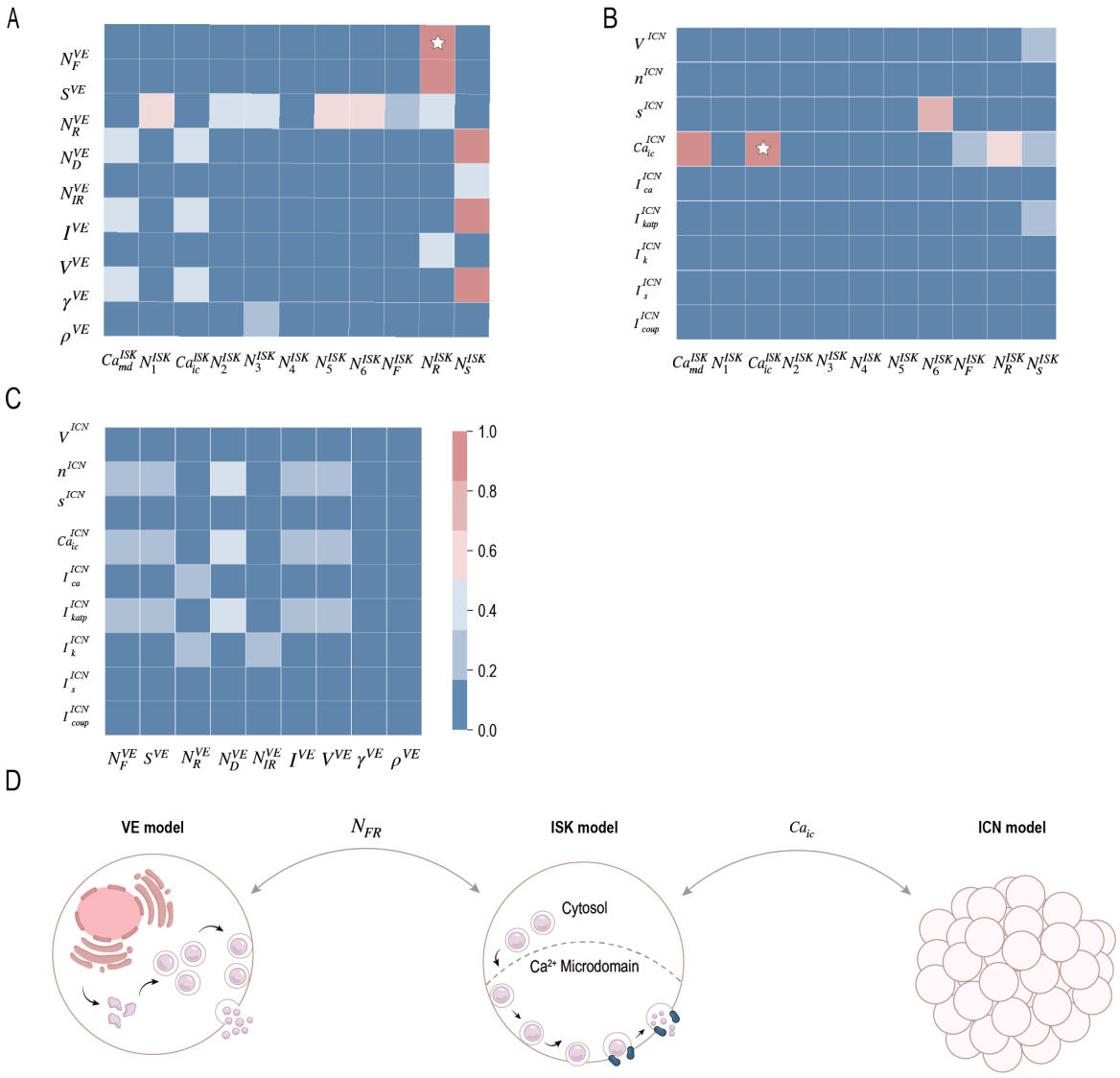

Fig. S2 (A-C) Selection of connecting variables based on the Pearson coefficient analysis. White stars indicate two sets of selected connecting variables: the number of insulin vesicles fused with membrane in VE model, N_F^{VE}, and those in the releasable state in ISK model, N_R^{ISK}; the intracellular Ca^{2+} levels in the ISK model, Ca_{ic}^{ISK} and the ICN model, Ca_{ic}^{ICN} models. (D) Coupling among three models by introducing two coupling variables, N_{FR} and Ca_{ic}, to statistically relate the two sets of connecting variables, respectively. Gray arrows indicate the flow of information between the coupled models.

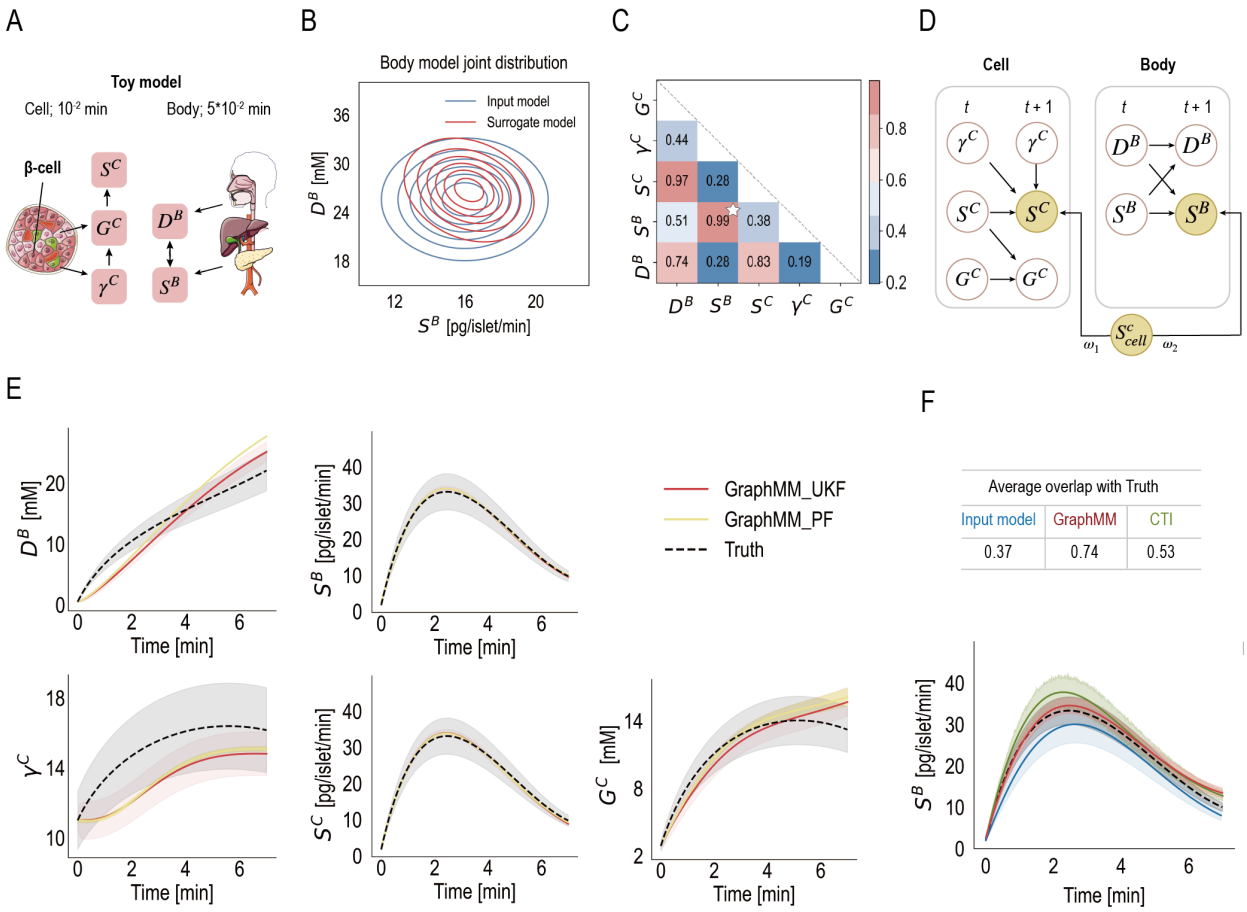

Fig. S3 (A) Schematic representation of the toy model, comprising a cell system (10^{-2} min) and a body system ($5 * 10^{-2}$ min). (B) Joint distribution of the input body model (blue dashed line) and its corresponding surrogate model (red solid line). (C) Selection of connecting variables between the cell and body models based on the Pearson coefficient analysis. White star indicates the selected connecting variables: the insulin secretion rates in the cell model S^C and in the Body model S^B. (D) Meta PGM graph over the cell and body surrogate models. (E) Time courses of all five variables in the synthetic metamodel. The comparison includes predictions of the metamodel constructed using GraphMM and infered using Unscented Kalman Filters (UKF, blue solid line) and Particle Filters (PF, orange solid line), and the Truth (black dashed line). The comparison includes the input model (dashed orange line), surrogate model (blue solid line), updated surrogate model (red solid line), and the Truth (black solid line). Shaded regions represent standard deviations (SDs). (F) Overlap of model variable distributions with the Truth, averaged across all variables and time courses. The comparison includes the input model, the metamodel constructed using GraphMM, and the metamodel constructed using a common timescale integration (CTI) approach. An example time course of the insulin secretion rate in the body model, S^B, is shown for the Truth (black solid line), input model (blue dashed line), metamodel using GraphMM (red solid line), and metamodel using CTI (green solid line).

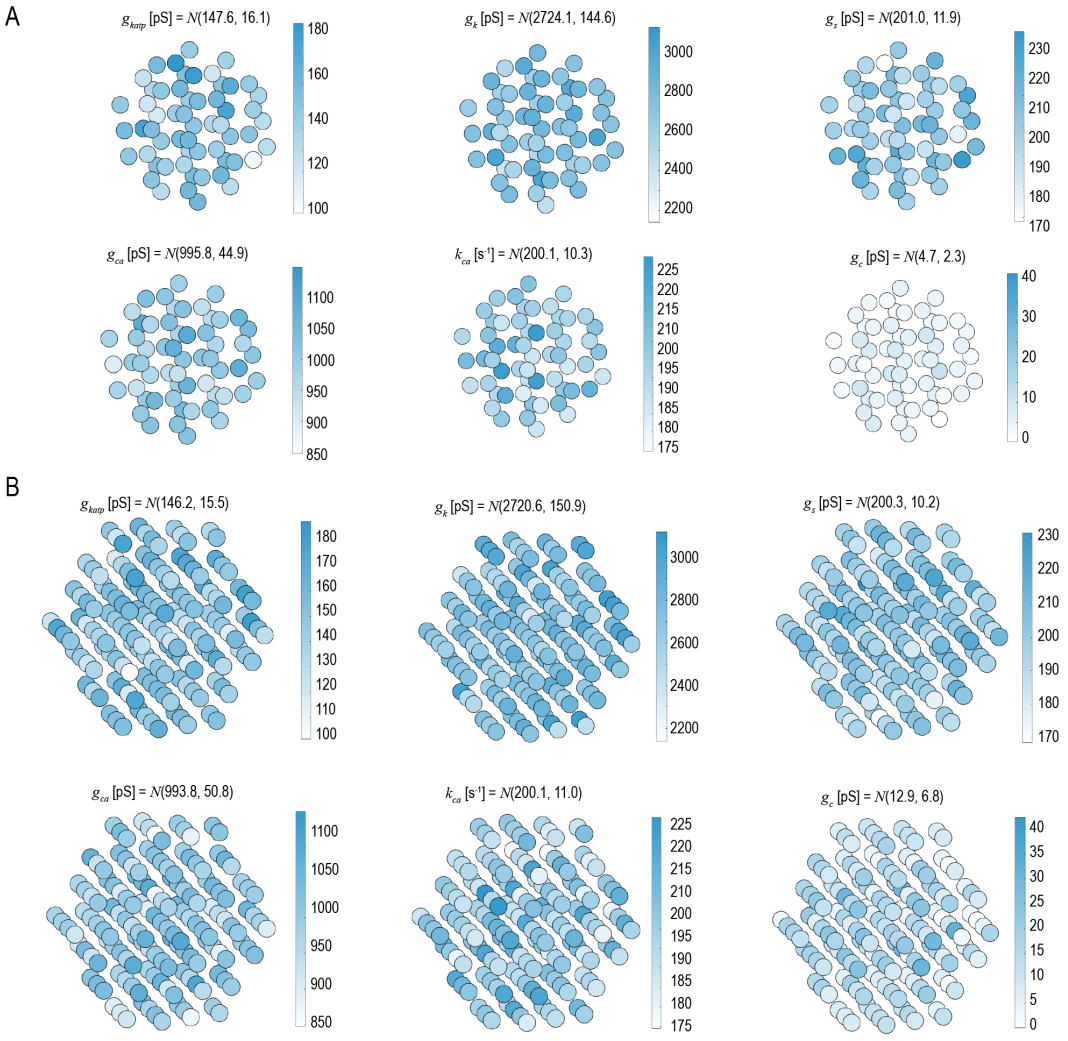

Fig. S4 Ion channel and gap junction conductance of Metamodel-57 and Metamodel-153. The conductance values for various ion channels and gap junctions include: ATP/ADP-dependent potassium channel conductance, g_{katp}, voltage-gated potassium channel conductance, g_k, slow inhibitory potassium channel conductance, g_s, voltage-gated Ca^{2+} channel conductance, g_{ca}, calcium pump rate, k_{ca}, and gap junction conductance, g_c.

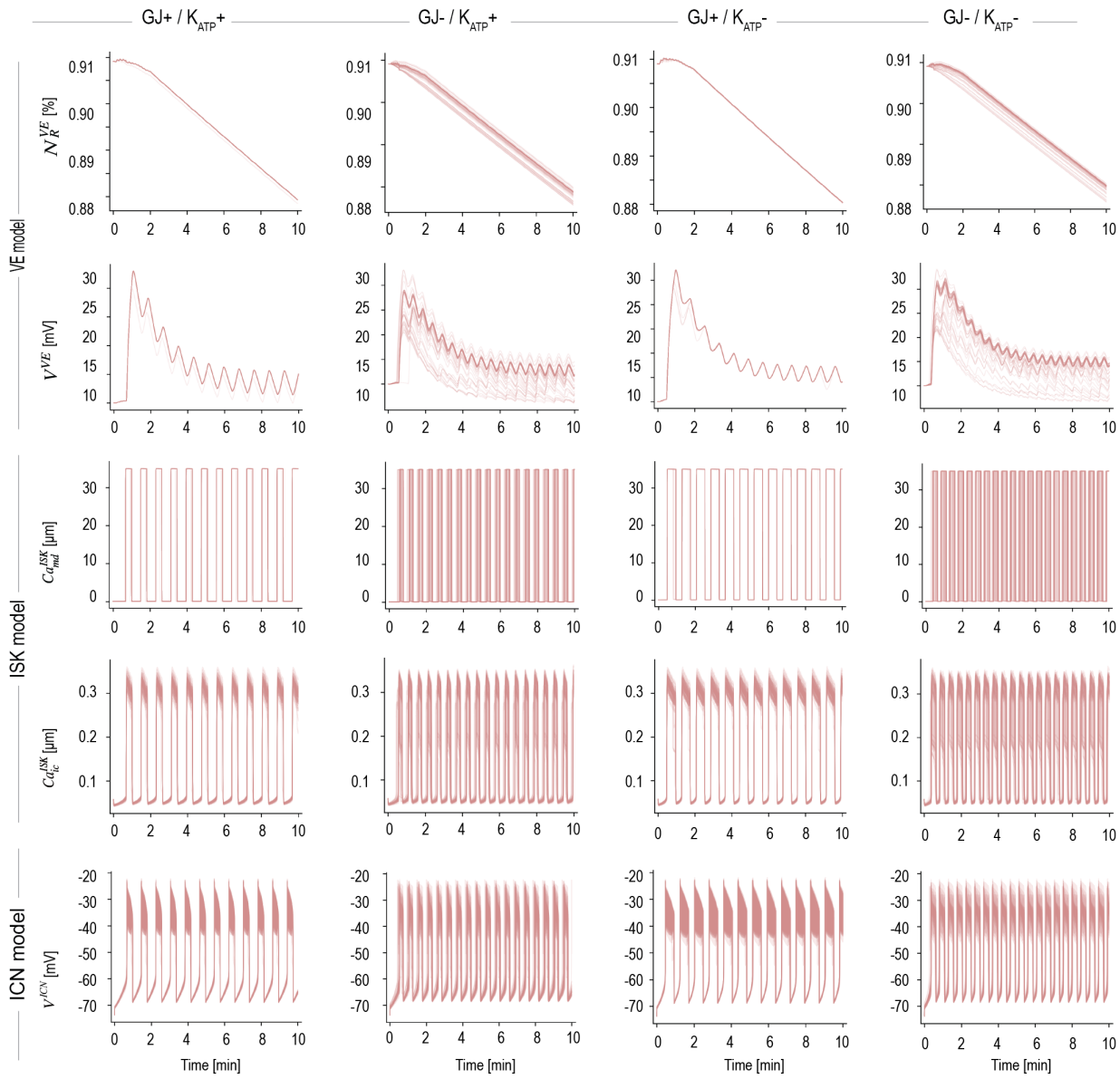

Fig. S5 Metamodel predictions across molecular, cellular and islet scales under four intercellular communication conditions: GJ+/K$_{ATP}$+, GJ-/K$_{ATP}$+, GJ+/K$_{ATP}$-, and GJ-/K$_{ATP}$. Predictions include the fraction of insulin vesicles in the reserve pool N_R^{VE}, the pool of vesicle membrane materials V^{VE}, the Ca^{2+} concentration in the microdomain Ca_{md}^{ISK}, the cytosolic Ca^{2+} concentration Ca_{ic}^{ISK}, and the membrane potential of each cell V^{ICN} for all β-cells in the islet network.

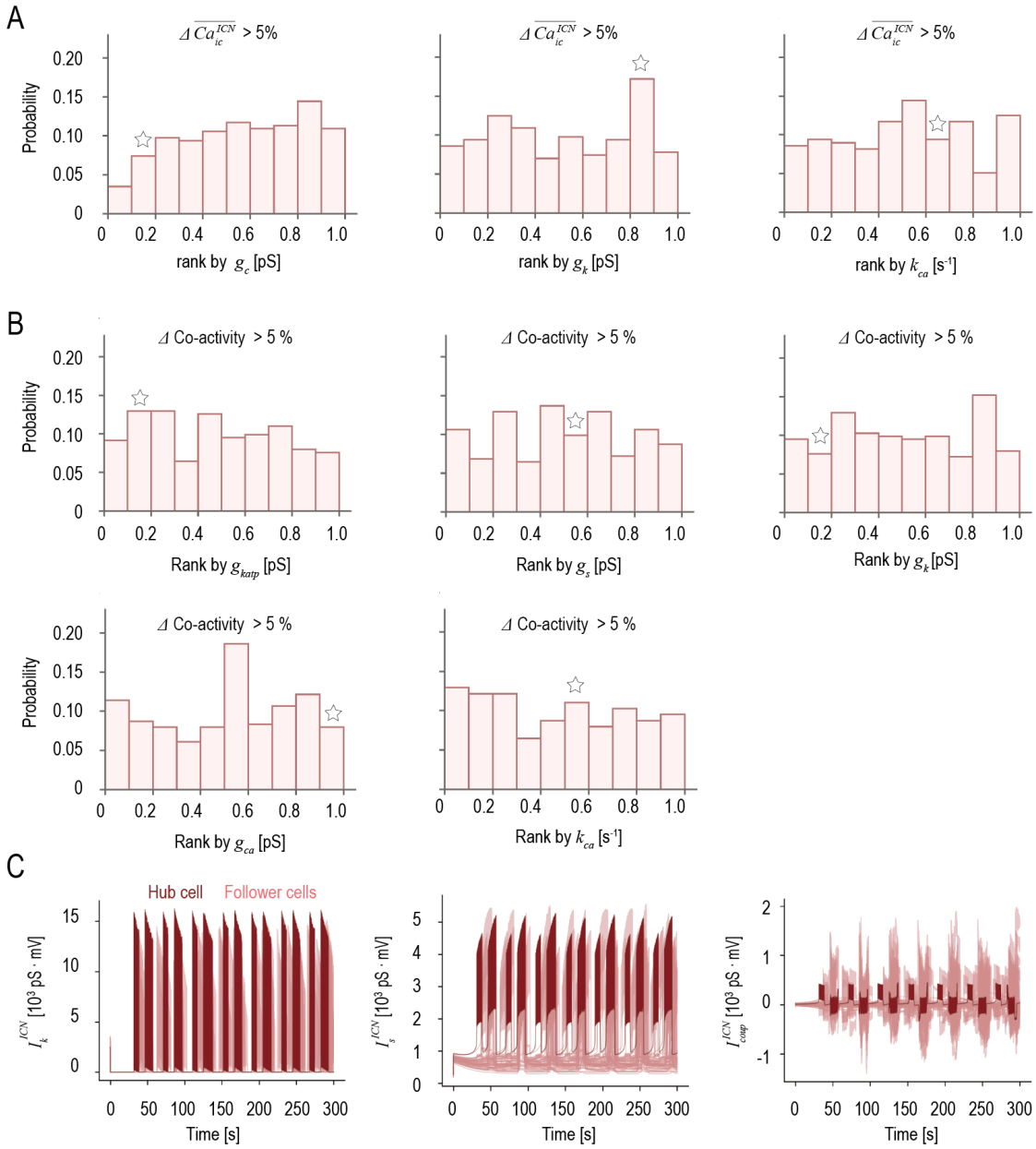

Fig. S6 (A) Rank of ion channel conductance in hub cells driving islet activity relative to all other islet cells, with a score of 1 indicating the highest conductance and 0 the lowest. Shown are gap junction conductance, g_c, voltage-gated potassium channel conductance, g_k, and calcium pump rate, k_{ca}. (B) Rank of ion channel conductance in hub cells driving islet synchronization relative to all other islet cells. Shown are voltage-gated potassium channel conductance, g_k, slow inhibitory potassium channel conductance, g_s, voltage-gated potassium channel conductance, g_k, voltage-gated Ca^{2+} channel conductance, g_{ca} and calcium pump rate, k_{ca}. (C) Ion channel currents of each β-cell in the islet, with the dark red curve corresponding to the hub cell 11. Shown are voltage-gated potassium current, I_k^{ICN}, slow inhibitory potassium current, I_s^{ICN}, and gap junctional passive coupling current , I_{coup}^{ICN}.

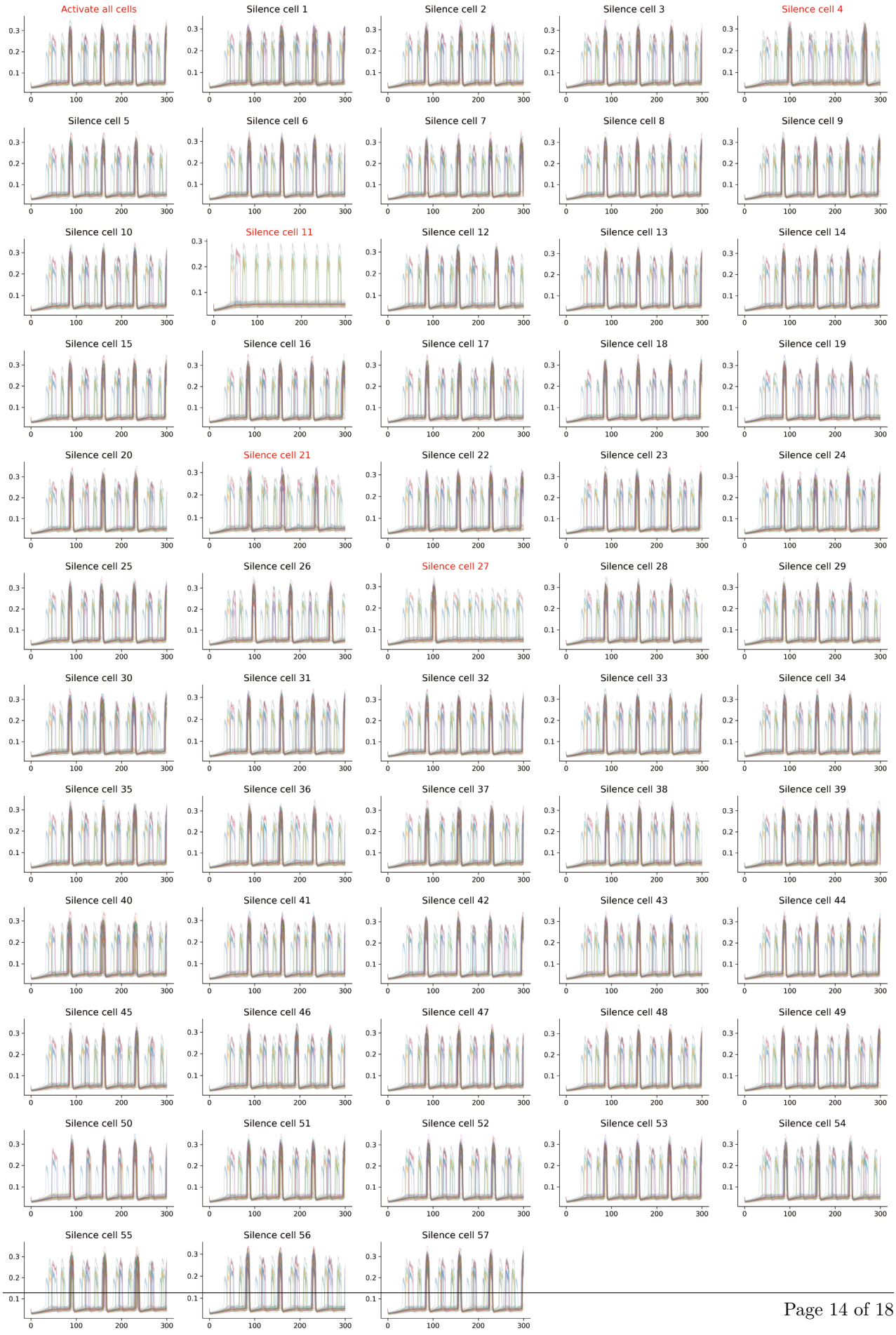

Fig. S7 Time courses of intracellular Ca^{2+} levels, Ca_{ic}^{ICN}, of individual β-cells in the islet network under two conditions: activate all cells and silence individual cells. Highlighted in red are conditions including: activating all cells; silencing cell 11, which significantly reduces β-cell activity; silencing cells 21 and 27, which moderately reduce *beta*-cell activity; and silencing other cells, such as cell 35, which has negligible effects

Supplementary Tables

Table S1 Variables and parameters of the Vesicle Exocytosis (VE) model

Model variables:		
Name	Description	Unit
I	Pool of proinsulin aggregates	-
V	Pool of granule membrane material	-
N_F	Insulin secretion rate of a pancreas	-
N_R	Number of vesicles in the reserve pool	-
N_D	Number of vesicles in the pool of docked vesicles	-
N_{IR}	Number of vesicles in the pool of immediately releasable vesicles	-
γ	Rate coefficient of granule externalization and priming	/min
Φ	Oscillatory forcing function that represents the events inducing [ATP] oscillations	-
ρ	Rate coefficient of granule fusion with cell membrane	/min
G	Glucose concentration	mM
h_γ	Glucose activation	-
h_ρ	The action of [ATP] on Ca^{2+}	-
S	Insulin secretion rate	pM/min
Model parameters:		
k	Rate of formation of proinsulin-containing vesicles	/min
α_I	Rate of degradation of proinsulin aggregates	/min
b_I	Biosynthesis rate of proinsulin aggregates	/min
α_v	Rate of degradation of granule membrane material	/min
b_v	Rate of biosynthesis of granule membrane material	/min
σ	Rate of insulin release from vesicles fused with cell membrane	/min
τ_v	Time delay related to recycling of granule membrane material	min
k_1^+	Rate of association for the binding between vesicle and Ca channel	/min
k_1^-	Rate of dissociation for the binding between vesicle and Ca channel	/min
C_T	Pool of total Ca channels	-
η	Rate in the equation for γ	/min
γ_b	Basal rate coefficient of granule externalization and priming	/min
ϵ	Rate constant in the equation for ρ	/min
$\hat{h}$	Maximal value of h_γ	/min
τ_G	Time delay related to time required by glucose metabolism for activation of γ	min
$\hat{G}$	Glucose concentration over which h_γ remains constant	mM
G^*	Glucose concentration threshold for the activation of γ	mM
I_0	Insulin amount contained in a granule	amol
k_ρ	Parameter representing the sensitivity of ρ on the activatory action of γ	amol

Table S2 Variables and parameters of the Insulin Secretion Kinetic (ISK) model

Model variables:		
Name	Description	Unit
Ca_{md}	Microdomain Ca^{2+} concentration	mM
Ca_{ic}	Cytosol Ca^{2+} concentration	mM
J_L	Molar Ca^{2+} influx through open L-type Ca^{2+} channels	μM/s
J_R	Molar Ca^{2+} influx through open R-type Ca^{2+} channels	μM/s
N_1	Number of primed vesicles inside the microdomain	-
N_2	Number of bounded vesicles	-
N_3	Number of triggered vesicles	-
N_4	Number of pre-fused vesicles	-
N_5	Number of primed vesicles outside the microdomain	-
N_6	Number of vesicles just arrived from reserve pool	-
N_F	Number of fused vesicles	-
N_R	Number of releasing vesicles	-
N_S	Number of secreted vesicles	-
S	Insulin secretion rate	mM/min
Model parameters:		
Name	Description	Unit
f_{md}	Ratio of the free to the bound Ca^{2+} in the microdomain compartment	-
fi	Ratio of the free to the bound Ca^{2+} in the cytosol compartment	-
B	Transport rate of Ca^{2+} between the two compartments	-
f_v	Ratio of the compartmental volume of the microdomain to that of the cytosol	-
α	Constant factor that converts the current into the mole flux of Ca-ions	-
v_{cell}	Volume of the cell	pl
v_{md}	Volume of the microdomain compartment	fl
k_1	Rate coefficient	/μM/s
k_{-1}	Rate coefficient	/s
r_1	Rate coefficient	/s
r_{-1}	Rate coefficient	/s
r_2	Rate coefficient	/s
r_{-2}	Rate coefficient	/s
r_3	Rate coefficient	/s
r_{-3}	Rate coefficient	/s
μ_1	Rate coefficient	/s
μ_2	Rate coefficient	/s
μ_3	Rate coefficient	/s

Table S3 Variables and parameters of the Islet Cell Network (ICN) model

Model variables:		
Name	Description	Unit
V_i	Membrane potential of each cell i	mV
I_{katp}	ATP/ADP ratio dependent potassium current	pS $\cdot mV$
I_{ca}	Voltage-dependent calcium current	pS $\cdot mV$
I_k	Voltage-gated potassium current	pS $\cdot mV$
I_s	Slow inhibitory potassium current	pS $\cdot mV$
I_{coup}	Passive coupling current	pS $\cdot mV$
I_{cl}	Passive chloride current	pS $\cdot mV$
n_i	Voltage gated potassium channel gating variable of each cell i	-
s_i	Slow inhibitory potassium channel gating variable of each cell i	-
Ca_i	Intracelluar Ca^{2+} concentration of each cell i	μM
Model parameters:		
Name	Description	Unit
k_{ca}	Ca^{2+} pump rate	pS
g_{katp}	ATP/ADP dependent potassium channel conductance	pS
g_{ca}	Voltage-gated Ca^{2+} channel conductance	pS
g_k	Voltage-gated potassium channel conductance	pS
g_s	Slow inhibitory potassium channel conductance	pS
g_c	Gap junction conductance	-75 mV
V_k	Potassium Nernst potential	25 mV
V_{ca}	Calcium Nernst potential	-70 mV
V_{cl}	Chloride Nernst potential	pS
N_{cell}	Number of cells per islet	-